Remote Sensing of Environment 115 (2011) 3647–3658

Contents lists available at SciVerse ScienceDirect

Remote Sensing of Environment

journal homepage: www.elsevier.com/locate/rse

Development and evaluation of SST algorithms for GOES-R ABI using MSG SEVIRI as a proxy

B. Petrenko [a,b,*], A. Ignatov [a], N. Shabanov [a,b], Y. Kihai [a,c]

[a] NOAA/NESDIS, Center for Satellite Applications and Research, Camp Springs, Maryland, United States
[b] IMSG Inc., Kensington, Maryland, United States
[c] Dell Perot Government Systems, Fairfax, Virginia, United States

ARTICLE INFO

Article history:
Received 18 February 2011
Received in revised form 29 August 2011
Accepted 6 September 2011
Available online 20 October 2011

Keywords:
Sea surface temperature
MSG SEVIRI
GOES-R ABI
Regression
Optimal Estimation

ABSTRACT

Cross-evaluation of sea surface temperature (SST) algorithms was undertaken using split-window channels of Meteosat Second Generation Spinning Enhanced Visible and Infrared Imager (SEVIRI) as a proxy for the Geostationary Operational Environmental Satellites-R (GOES-R) Advanced Baseline Imager (ABI). The goal of the study was to select the algorithm which provides the highest and the most uniform SST accuracy within the area observed by the geostationary sensor. The previously established algorithms, such as Non-Linear Regression (NLR) and Optimal Estimation (OE) were implemented along with two new algorithms, Incremental Regression (IncR) and Corrected Non-Linear Regression (CNLR), developed within preparations for the GOES-R ABI mission. OE, IncR and CNLR adopt the first guesses for SST and brightness temperatures (BT) and retrieve deviations of SST from the first guess (increments). OE retrieves SST increments with inversion of the radiative transfer model, whereas CNLR and IncR use regression equations. The difference between CNLR and IncR is that CNLR uses NLR coefficients, whereas IncR implies optimization of coefficients specifically for incremental formulation. Accuracy and precision of SST retrievals were evaluated by comparison with drifting buoys. The major observations from this study are as follows: 1) all algorithms adopting first guesses for SST and BTs are capable of improving SST accuracy and precision over NLR; and 2) IncR delivers the highest overall SST precision and the most uniform distributions of regional SST accuracy and precision. This paper also addresses implementation and validation issues such as bias correction in simulated BTs; preserving sensitivity of incremental SST retrievals to true SST variations; and selection of criteria for optimization and validation of incremental algorithms.

1. Introduction

Sea surface temperature (T_S, SST; see Tables 1 and 2 for list of abbreviations and notations used in the paper), derived from satellite observations of top-of-the atmosphere thermal infrared radiation, is used in many environmental applications. SST retrievals from geostationary platforms such as Meteosat Second Generation (MSG — e.g., Schmetz et al., 2002) and Geostationary Operational Environmental Satellites (GOES — e.g., Maturi et al., 2008; Wu et al., 1999) benefit from continuous observations of a vast ocean area over the full diurnal cycle. Another aspect of a geostationary sensor is that each individual element on the earth's surface within the observed area is viewed at a nearly constant view zenith angle (VZA, θ). This emphasizes the need for taking special care to ensure uniformity of accuracy and precision of SST retrievals within a wide range of VZA, compared with polar-orbiting sensors.

SST will be one of the key products of the Advanced Baseline Imager (ABI, e.g., Schmit et al., 2005) scheduled for launch in 2015 onboard the new generation GOES-R series. In 2005, NOAA formed the GOES-R Algorithm Working Group (AWG) to ensure that a full suite of algorithms is developed and tested on proxy data and is available for product generation from ABI shortly after the launch. The SST Application Team, which is a part of the GOES-R AWG, has proposed implementation and cross-evaluation of prospective SST algorithms within a consistent framework, using the Advanced Very High Resolution Radiometer (AVHRR) onboard polar-orbiting NOAA and MetOp satellites and the Spinning Enhanced Visible and Infrared Imager (SEVIRI) onboard the geostationary MSG satellites as ABI proxies. This study began with implementation of existing SST algorithms, such as regression (e.g., McClain et al., 1985; Walton et al., 1998) and radiative transfer model (RTM) — based Optimal Estimation (OE — e.g., Rodgers, 1976) and eventually has led to development of the Hybrid or Incremental Regression (IncR) algorithm, which is aimed at combining the advantages of both approaches (Ignatov et al., 2010; Petrenko et al., 2010b). This paper describes the results of implementation and cross-evaluation of SST algorithms using Meteosat-9 SEVIRI data.

* Corresponding author at: Room 601-4, 5200 Auth Rd., Camp Springs, MD, 20746, United States. Tel.: +1 301 763 8348x360; fax: +1 301 763 8572.
E-mail address: boris.petrenko@noaa.gov (B. Petrenko).

0034-4257/$ – see front matter © 2011 Elsevier Inc. All rights reserved.
doi:10.1016/j.rse.2011.09.003

Table 1
List of abbreviations.

ABI	Advanced Baseline Imager
ACSM	ACSPO Clear-Sky Mask
ACSPO	Advanced Clear-Sky Processor for Oceans
AVHRR	Advanced Very High Resolution Radiometer
AWG	Algorithm Working Group
BT	Brightness temperature
CNLR	Corrected Non-Linear Regression
CRTM	Community Radiative Transfer Model
MDB	Matchup Database
DSST	Daily High-Resolution Blended SST
ESD	Estimated SST Error Standard Deviation
ECMWF	European Center for Medium-range Weather Forecasting
GFS	Global Forecast System
GOES	Geostationary Operational Environmental Satellites
*i*Quam	In situ SST Quality Monitor
IncR	Incremental Regression
LUT	Lookup table
MSG	Meteosat Second Generation
NCEP	National Centers for Environmental Prediction
NESDIS	National Environmental Satellite, Data and Information Service
NLR	Non-Linear Regression
NOAA	National Oceanic and Atmospheric Administration
NWP	Numerical Weather Prediction
ODSF	Optical Depth Scaling Factor
OE	Optimal Estimation
OSTIA	Operational Sea Surface Temperature and Sea Ice Analysis
RTM	Radiative transfer model
RTTOVS	Radiative Transfer for TIROS Operational Vertical Sounder
SD	Standard deviation
SEVIRI	Spinning Enhanced Visible and Infrared Imager
SNR	Signal-to-Noise Ratio
SST	Sea surface temperature
TPW	Total Precipitable Water Vapor Content
VZA	View zenith angle

Table 2
List of notations.

T_S	SST
T_S^0	First guess SST
T_S^i	SST measured in situ
T_B	Observed BT
T_{B11}	Observed BT in 11 μm channel
T_{B12}	Observed BT in 12 μm channel
T_B^0	First guess brightness temperature
T_{B11}^0	First guess BT in 11 μm channel
T_{B12}^0	First guess BT in 12 μm channel
T_B^{CRTM}	BT simulated with CRTM
a_0	NLR offset
$\mathbf{a}=[a_1, a_2, a_3]^T$	Vector of NLR coefficients
b_0	IncR offset
$\mathbf{b}=[b_1,b_2, b_3]^T$	Vector of IncR coefficients
b_{0LS}	IncR offset
$\mathbf{b_{LS}}$	Vector of IncR coefficients calculated with the least-squares method
$\mathbf{Y}$	Vector of regressors, constructed from observed BTs
$\mathbf{Y^0}$	Vector of regressors, constructed from first guess BTs
θ	Satellite view zenith angle
W	Total column water vapor content in the atmosphere
M	Bias in retrieved SST
σ	Standard deviation of retrieved SST
r	Incremental correlation coefficient
M_B	Bias in $T_B-T_B^{CRTM}$
τ	Optical depth of water vapor absorption
τ_0	A priori estimate of water vapor absorption
β	ODSF
$\mathbf{z}$	Vector of variables retrieved with OE
$\mathbf{z^0}$	A priori value of $\mathbf{z}$
$\mathbf{S}$	A priori covariance matrix of $\mathbf{z}$
$\mathbf{\Delta}$	Covariance matrix of radiometric noise
$\mathbf{K}$	Jacobian
η	Multiplication factor at S^{-1} in OE equation
σ_{SST}	A priori SD of SST
σ_β	A priori SD of ODSF
σ_{cell}	Regional average SD of retrieved SST minus DSST

At present, the majority of operational SST products are generated using regression algorithms. Although the forms of regression SST equations are devised to decouple SST variations from variations in atmospheric transmission and emission, residual atmospheric effects can cause significant regional biases in retrieved SST. For SEVIRI, these biases were explored by Merchant et al. (2009a) and Le Borgne et al. (2011). The OE and IncR algorithms represent an alternative approach to SST retrieval, which can be defined as "incremental". This approach implies adopting the first guesses for SST, T_S^0, from SST analysis fields and first guesses T_B^0 for observed brightness temperatures (BT, T_B) from RTM simulations. Given T_S^0 and T_B^0, the task of the incremental algorithms is to retrieve SST increments, $T_S-T_S^0$, from BT increments, $T_B-T_B^0$, rather than T_S from T_B. Along with selection of the algorithm which provides the highest and most uniform SST accuracy and precision within the area observed by a geostationary sensor, the objective of this study was to gain experience in implementation and validation of incremental SST algorithms.

The SST algorithms were implemented within the Advanced Clear-Sky Processor for Oceans (ACSPO), initially developed at the National Environmental Satellite Data and Information Service (NESDIS) to generate clear-sky radiances, SST, and aerosols from the AVHRR sensors onboard NOAA and MetOp satellites (Liang & Ignatov, in press; Liang et al., 2009; Petrenko et al., 2010a) and later adopted for MSG SEVIRI (Shabanov et al., 2009, 2010). The regression-based ACSPO SST algorithms are trained against buoy measurements without correction for the thermal skin effect. ACSPO enables on-line simulations of clear-sky BTs using the Community Radiative Transfer Model (CRTM, Han et al., 2005; Liang et al., 2009) with analysis SST and Numerical Weather Prediction (NWP) atmospheric fields as input. In this study, CRTM version 1.1 is used in conjunction with the AVHRR-based 0.25° Daily High-Resolution Blended SST analysis (DSST, Reynolds et al., 2007) and the 6-hour 1° atmospheric forecast fields from the National Centers for Environmental Prediction (NCEP) Global Forecast System (GFS, available at http://nomad3.ncep.noaa.gov/pub/gfs/rotating/). The DSST field is anchored to buoy and ship SST, and thus it is expected to be consistent with ACSPO regression algorithms, which are also trained against in situ measurements. CRTM BTs, T_B^{CRTM}, are computed on the GFS grid and interpolated in space and time to the sensor's pixels. Similar interpolation is applied to selected GFS atmospheric variables, such as Total Precipitable Water Vapor Content in the atmosphere (TPW, W). The pixel-level first guess SST is produced by spatial interpolation of DSST. The ACSPO also incorporates Clear-Sky Mask (ACSM) — the module that identifies clear-sky ocean pixels suitable for SST retrieval (Petrenko et al., 2010a). The ACSPO infrastructure allows implementation and testing, in a real-time setting, of SST algorithms based both on regression and on CRTM simulations.

Split-window SEVIRI Channels 9 and 10, centered at 10.8 μm and 12 μm, were used in this study as the proxies of the ABI channels 14 and 15, centered at 11.2 μm and 12.3 μm. Note that since the spectral responses for SEVIRI and ABI channels are different, the performance of SST algorithms reported in this study for SEVIRI can be different from that for the future ABI sensor. The SEVIRI Channel 4, centered at 3.9 μm, was not used because our initial analyses (Shabanov et al., 2009), consistent with Le Borgne et al. (2011), have shown that this SEVIRI channel does not improve the accuracy of nighttime SST retrievals but introduces inconsistency between daytime and nighttime retrievals.

2. SST algorithms

In this Section, the SST algorithms implemented for this study are briefly reviewed. More implementation details are provided in Sections 5 and 6.

2.1. Non-Linear Regression (NLR)

The split-window Non-Linear Regression (NLR, Walton et al., 1998) was implemented for SEVIRI in the same form as used in ACSPO for operational processing of AVHRR data (e.g., Petrenko et al., 2010a):

$$T_S = a_0 + \mathbf{a}^{\mathrm{T}}\mathbf{Y}, \tag{1}$$

$$\mathbf{Y} = \left[T_{B11}, (T_{B11}-T_{B12})\left(T_S^0-273.15\right), (T_{B11}-T_{B12})(sec\,\theta-1)\right]^{\mathrm{T}}. \tag{2}$$

Here, $\mathbf{Y}$ is a vector of regressors, a_0 is an offset, and $\mathbf{a}=[a_1, a_2, a_3]^{\mathrm{T}}$ is a vector of regression coefficients, $[*]^{\mathrm{T}}$ denotes vector transposition. T_{B11} and T_{B12} are BTs observed at 10.8 μm and 12 μm. The regression coefficients are derived from matchups of T_B with in situ SST, T_S^i. Alternative implementations of NLR may use different forms of equations and use coefficients derived from RTM simulations (e.g. Brisson et al., 2002; Le Borgne et al., 2011).

2.2. Corrected Non-Linear Regression (CNLR)

Ignatov et al. (2010) and Le Borgne et al. (2011) suggested estimation of regional bias in NLR SST by subtracting T_S^0 from Eq. (1), in which observed BTs are replaced with their simulated first guesses:

$$M = a^0 + \mathbf{a}^{\mathrm{T}}\mathbf{Y^0} - T_S^0, \tag{3}$$

$$\mathbf{Y}^0 = \left[T_{B11}^0, (T_{B11}^0-T_{B12}^0)(T_S^0-273.15), (T_{B11}^0-T_{B12}^0)(sec\theta-1)\right]^{\mathrm{T}}. \tag{4}$$

Here, T_{B11}^0 and T_{B12}^0 are first guesses for T_{B11} and T_{B12}. Subtracting Eq. (3) from Eq. (1) produces the Corrected NLR (CNLR) SST estimate:

$$T_S = T_S^0 + \mathbf{a}^{\mathrm{T}}\left(\mathbf{Y}-\mathbf{Y^0}\right). \tag{5}$$

CNLR SST deviates less from T_S^0 and fits T_S^i more precisely than NLR SST (e.g., Le Borgne et al., 2011). Given the NLR coefficients, the CNLR does not require further adjustment. CNLR can be considered an intermediate algorithm between conventional and incremental approaches because it retrieves SST increments, but does so with NLR coefficients derived from matchups of T_B with T_S^i. However, NLR coefficients can be suboptimal for incremental retrieval.

2.3. Incremental Regression (IncR)

The Incremental Regression (IncR) algorithm, developed during preparations for the GOES-R ABI mission (Ignatov et al., 2010; Petrenko et al., 2010b), implies optimization of regression specifically for retrieval of SST increments. In general, the IncR can involve selection of regressors most suitable for incremental retrieval and derivation of regression coefficients from matchups of $T_B-T_B^0$ with $T_S^i-T_S^0$. In this study, we have chosen to focus on the effect of optimization of coefficients, keeping for IncR the incremental form of the NLR Eq. (1):

$$T_S = T_S^0 + b_0 + \mathbf{b}^{\mathrm{T}}\left(\mathbf{Y}-\mathbf{Y^0}\right). \tag{6}$$

Here, b_0 is an offset, and $\mathbf{b}=[b_1,b_2,b_3]^{\mathrm{T}}$ is a vector of regression coefficients. Eq. (6) is similar to Eq. (5) with the exception that Eq. (6) includes an offset and its coefficients are derived from matchups of $(T_B-T_B^0)$ with $(T_S^i-T_S^0)$. Cross-evaluation of NLR, CNLR and IncR algorithms thus allows sequential demonstration of the effect of replacing conventional NLR Eq. (1) with its incremental analog Eq. (5) and the effect of replacing NLR coefficients in CNLR with optimized coefficients in IncR.

2.4. Optimal Estimation (OE)

OE (e.g., Rodgers, 1976) was the first incremental technique applied to SST retrieval from AVHRR (Gemmill et al., 2007; Merchant et al., 2008) and from SEVIRI (Merchant et al., 2009a). Being based on inversion of RTM, OE performs the atmospheric correction in a different way than regression algorithms. While regression accounts for atmospheric effects in some "global average" sense, by selecting regressors and deriving coefficients from the full Matchup Database (MDB), OE attempts to account for local deviations of atmospheric transmission and emission from those simulated with RTM and NWP data, by simultaneous retrieval of SST and atmospheric state variables. Since the number of simultaneously retrieved variables cannot exceed the number of channels used, only one atmospheric variable can be retrieved along with SST from two split-window channels. Implementation of OE for SST involves low-dimensional parameterization of RTM, calculation of RTM Jacobian, explicit specification of a priori statistical distribution for unknown variables, and inversion of a set of RTM equations in each pixel. As a result, OE is more computationally expensive than regression-based algorithms, and its implementation is more ambiguous and less straightforward. One of the goals of OE implementation within this study was to verify that the increased volumes of computations and implementation complexities are justified by improvement in SST accuracy and precision.

3. Criteria for optimization and validation of SST algorithms

Every SST algorithm exploits specific approximation of the inverse relationship between SST and observed BTs. Accuracy and precision of these approximations can vary for different algorithms. In addition, the performance statistics can degrade in time due to long-term calibration trends and non-uniform accuracy of auxiliary data. Here, we explore the intrinsic capabilities of SST algorithms to fit in situ SST using the same MDB of SEVIRI and buoy observations for both optimization and validation of SST algorithms. This way, we leave aside possible effects of instability of the sensor and variable accuracy of NWP atmospheric data used as input for CRTM. The long-term trends in SST retrieval accuracy and precision will be a subject of a future work.

The SST algorithms were optimized and cross-evaluated using SEVIRI observations taken at 30-minute intervals during 1–30 June 2008 within the geographical area (retrieval domain) from 60°S to 60°N and 60°W to 60°E excluding the region from 10°N to 30°N and 10°W to 30°W, in which SEVIRI SST retrievals often show significant negative biases due to the effect of Saharan dust (e.g., Merchant et al., 2006). Although in general Saharan dust can spread over much wider area (e.g., Swap et al., 1996), this 20°×20° region was excluded from consideration based on visual analyses of nighttime SEVIRI SST images taken in June 2008. Only nighttime pixels with solar zenith angle greater than 90° and identified as "clear-sky" by the ACSM were used in this study. Daytime observations were excluded from the analysis to avoid distortions of BTs and SST by non-uniform diurnal warming patterns (e.g., Kawai & Wada, 2007; Minnett, 2003) and potential sun glint contamination (e.g., Khattak et al., 1991) on the ocean surface. Another reason to exclude daytime observations from consideration is that the difference between "skin" SST within the upper ~10 μm layer, to which the SEVIRI observations are sensitive, and in situ SST, measured at ~1 m depth, is largest in the daytime (e.g., Donlon et al., 2002). The MDB was formed by matching SEVIRI data with quality-controlled drifting buoy measurements selected with the in situ SST Quality Monitor (*i*Quam, Xu & Ignatov, submitted for publication; the description of *i*Quam is also available at http://www.star.nesdis.noaa.gov/sod/sst/iquam). Additional criteria for selection of drifters were that the time difference between the SEVIRI image and in situ measurements is ≤15 min and that the distance

of a buoy from the nearest clear-sky pixel on the SEVIRI image, closest in time, ≤10 km (note that the size of the SEVIRI pixels is 4.8 km at nadir). The total number of matchups in the database is N = 30,398. In situ SST increments $T_S^i - T_S^0$ within the MDB show near-Gaussian distribution with a mean bias of −0.058 K and standard deviation (SD) of 0.338 K (recall that ACSPO produces the first guess SST T_S^0 by interpolation of 0.25° spatial resolution DSST to SEVIRI pixels). The fact that T_S^0 fits T_S^i more precisely than satellite SST retrievals (typical SD of retrieved SST with respect to T_S^i is ~0.5 K), is consistent with other analyses (e.g., Le Borgne et al., 2011; O'Carroll et al., 2008; Xu & Ignatov, 2010). Fig. 1 shows number of matchups within 10° bins of VZA and 10 kg/m^2 bins of TPW. The number of matchups varies from 10^2 to 10^4 per bin, thus allowing analysis of statistics of retrieved SST as functions of VZA and TPW.

The criteria used for optimization and validation of SST algorithms deserve special consideration. Customarily, accuracy and precision of regression SST retrieval are characterized with bias and SD of retrieved SST with respect to in situ SST:

$$M\left(T_S - T_S^i\right) = \langle T_S - T_S^i \rangle, \tag{7}$$

$$\sigma\left(T_S - T_S^i\right) = \left\{ \left\langle \left[T_S - T_S^i - D\left(T_S - T_S^i\right) \right]^2 \right\rangle \right\}^{0.5}. \tag{8}$$

Here, $\langle x \rangle$ denotes averaging within the MDB — either over the entire retrieval domain or over specific geographical regions, or within VZA or TPW bins. Another important quantity which will be used in evaluation of incremental SST algorithms is SD of retrieved SST increment:

$$\sigma(T_S - T_S^0) = \left\{ \langle\langle [T_S - T_S^0 - M(T_S - T_S^0)]^2 \rangle\rangle \right\}^{0.5}, \tag{9}$$

$$M\left(T_S - T_S^0\right) = \langle\langle T_S - T_S^0 \rangle\rangle. \tag{10}$$

$\langle\langle x \rangle\rangle$ denotes averaging over clear-sky nighttime SEVIRI pixels from 1 to 30 June 2008.

Given the first guess SST T_S^0, the performance of SST algorithms can be also compared in terms of correlation r between retrieved and in situ SST increments:

$$r\left(T_S - T_S^0, T_S^i - T_S^0\right) = \left\langle \left[T_S - T_S^0 - M\left(T_S - T_S^0\right) \right] \left[T_S^i - T_S{}^0 - M\left(T_S^i - T_S{}^0\right) \right] \right\rangle / \left[\sigma\left(T_S - T_S{}^0\right) \sigma\left(T_S{}^i - T_S{}^0\right) \right], \tag{11}$$

$$M\left(T_S^i - T_S{}^0\right) = \left\langle T_S^i - T_S^0 \right\rangle, \tag{12}$$

$$\sigma\left(T_S^i - T_S^0\right) = \left\{ \left\langle \left[T_S^i - T_S^0 - M\left(T_S{}^i - T_S^0\right) \right]^2 \right\rangle \right\}^{0.5}. \tag{13}$$

In the regression analysis, the square of correlation r^2 (called coefficient of determination) represents "the proportion of the variability in the dependent variable that is explained by the independent variable" (e.g., Ostle & Malone, 1988). In our case, r^2 characterizes a contribution of variations in in situ SST increments to variations in retrieved SST increments, which are additionally disturbed by noise from factors such as variations in atmospheric transmission, radiometric noise, etc. Note that correlation between absolute T_S and T_S^i typically exceeds 0.99 and only slightly varies for different algorithms due to an overwhelming contribution of variations in T_S^0 to both T_S and T_S^i. In contrast, the correlation between the increments $T_S - T_S^0$ and $T_S^i - T_S^0$ (incremental correlation) is relatively low but distinguishably different for different SST algorithms. In this study, the incremental correlation is used as an additional measure of the relative performance of the SST algorithms.

Alternatively, a characteristic similar to r^2 can be obtained using RTM-based sensitivities of T_S to true SST, TPW, and other variables. These sensitivities can be calculated by substituting corresponding RTM derivatives into the algorithm's equation (Merchant et al., 2009b). However, this approach requires setting a joint statistical distribution of SST and other RTM variables, and calculation of RTM Jacobian with accuracy high enough to resolve the differences between the algorithms.

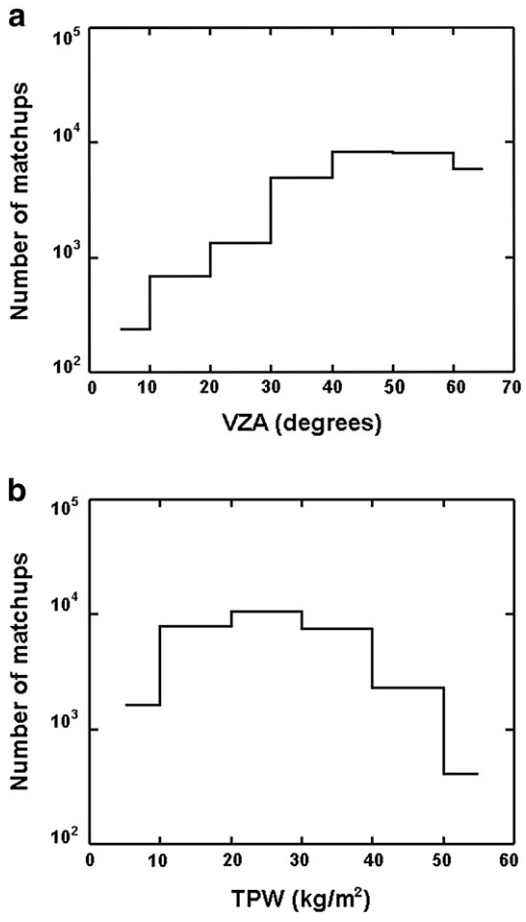

Fig. 1. Number of matchups in the database as a function of (a) VZA, binned at 10° and (b) TPW, binned at 10 kg/m^2.

4. Correction of biases in first guess brightness temperatures

BTs simulated with CRTM, T_B^{CRTM}, may be significantly biased with respect to observed BTs, T_B, due to modeling errors and incomplete (e.g., missing aerosol) or not fully accurate GFS or SST input fields. Observed BTs are also affected by uncertainties in calibration, spectral response functions, and residual cloud. Analyses of AVHRR observations (e.g., Liang et al., 2009; Petrenko et al., 2010a) have shown that the differences, $T_B - T_B^{CRTM}$, systematically deviate from zero and change in space and time. The dependencies of $T_B - T_B^{CRTM}$ biases on TPW, VZA and other variables are monitored for AVHRR on a daily basis at http://www.star.nesdis.noaa.gov/sod/sst/micros/ (Liang & Ignatov, in press). Similar monitoring for SEVIRI is currently under development. To prevent propagation of BT biases into estimated SST increments, these biases are usually corrected for, prior to using simulated BT as the first guess T_B^0. For the purpose of correction, BT bias is represented as a function of either geophysical variables, such as SST, TPW, and VZA, (e.g., Gemmill et al., 2007; Merchant et

al., 2008) or geographical coordinates (e.g., Le Borgne et al., 2011; Merchant et al., 2009a). Considering that BT bias is expected to be primarily a function of geophysical variables and that BT bias at any geographical point is sensitive to variations in local geophysical conditions, we adopted the former approach. The biases in $T_B - T_B^{CRTM}$ in channels 10.8 μm and 12 μm were represented as two-dimensional functions of (θ, W) by averaging $T_B - T_B^{CRTM}$ over all clear-sky nighttime SEVIRI pixels within $5° \times 5°$ kg/m^2 bins in June 2008. Because of essential nonlinearities, these functions were approximated with lookup tables (LUT). For any combination of θ and W, the value of bias, $M_B(\theta,W)$, was obtained by interpolation between the nearest LUT entries. The de-biased first guess BT was found for each pixel as:

$$T_B^0 = T_B^{CRTM} + M_B(\theta, W). \tag{14}$$

Fig. 2 shows that biases in $T_B - T_B^{CRTM}$ may exceed 1 K, and can significantly vary with VZA and TPW. Fig. 3 shows biases in $T_B - T_B^{CRTM}$ and $T_B - T_B^0$ averaged over nighttime clear-sky pixels within $10° \times 10°$ latitudinal/longitudinal cells in June 2008. Fig. 4 demonstrates TPW and VZA values averaged over the same cells. The most significant minima of $T_B - T_B^{CRTM}$ biases in Fig. 3, left panels, correspond to the lowest TPW values and the smallest VZA values consistently with dependencies shown in Fig. 2. Table 3 presents mean and SD of regional biases for $T_B - T_B^{CRTM}$ and $T_B - T_B^0$ averaged over all $10° \times 10°$ cells shown in Fig. 3. Fig. 3 and Table 3 suggest that the bias-corrected differences, $T_B - T_B^0$, are centered at zero and more uniform in space. The residual BT bias correction errors, which are likely due to regional variations in parameters other than TPW and VZA (e.g., residual cloud, aerosols, vertical profiles of water vapor and temperature), show themselves in still significant SD of $T_B - T_B^0$ in Table 3 and in noticeable variations in regional $T_B - T_B^0$ biases in Fig. 3, right panels. The SST algorithms are compared within this study and checked for sensitivity to a combination of various disturbing factors including the residual bias correction errors.

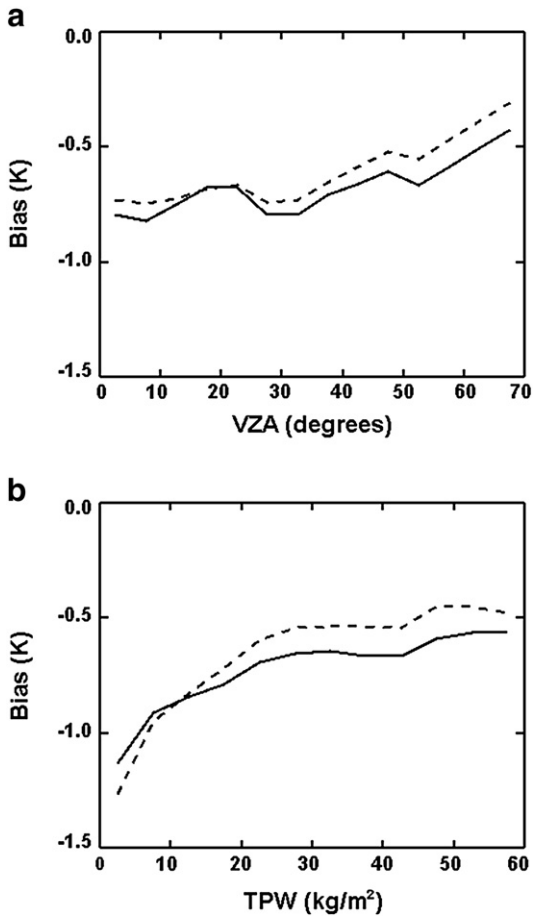

Fig. 2. Biases of SEVIRI−CRTM BT in (solid line) channels 10.8 μm and (dashed line) 12 μm as functions of (a) VZA and (b) TPW.

5. Derivation of NLR and IncR coefficients

NLR coefficients are derived from matchups of observed BTs and in situ SST using the least-squares method, by unconstrained minimization of the variance of retrieved SST from in situ SST over the full MDB:

$$\left\langle \left(a_0 - \mathbf{a}^{\mathbf{T}}\mathbf{Y} - T_S^i\right)^2 \right\rangle = \min. \tag{15}$$

A straightforward way to derive IncR coefficients for Eq. (6) would also be to find the "least squares" vector of coefficients $\mathbf{b_{LS}}$ and the offset b_{0LS} as a solution of the following unconstrained minimization problem:

$$\left\langle \left[T_S^i - T_S^0 - b_{0LS} - \mathbf{b}_{\mathbf{LS}}^{\mathrm{T}}\left(\mathbf{Y} - \mathbf{Y^0}\right)\right]^2 \right\rangle = \min. \tag{16}$$

However, the least-squares method, which works reasonably well for NLR, is not fully adequate for calculation of IncR coefficients. The least-squares method guarantees that biases in estimated regression coefficients are small only if errors in regressors are small compared with variations of the regressors (e.g., Ostle & Malone, 1988) — in other words, if Signal-to-Noise Ratio (SNR) for regressors is large enough. The SNR for incremental regressors $\mathbf{Y-Y^0}$ is much smaller than for NLR regressors $\mathbf{Y}$. Under clear-sky conditions, the global RMS variation in T_B is ~8 K, whereas the range of variations in $T_B - T_B^0$ is on the order of 0.5 K (e.g., Liang & Ignatov, in press; Liang et al., 2009; Petrenko et al., 2010a). Because of small SNR of incremental regressors, the least-squares method underestimates IncR coefficients. As a result, the IncR SST $T_S(\mathbf{b_{LS}})$, produced by substituting b_{0LS} and $\mathbf{b_{LS}}$ into Eq. (6), underestimates SST increments: SD of $T_S(\mathbf{b_{LS}}) - T_S^0$ averaged over the full retrieval domain during June 2008, $\sigma[T_S(\mathbf{b_{LS}}) - T_S^0]$, appears to be as small as 0.12 K. At the same time, $T_S(\mathbf{b_{LS}})$ also precisely fits T_S^i, with SD $\sigma[T_S(\mathbf{b_{LS}}) - T_S^i] = 0.32$ K, consistently with the fact that T_S^0 fits T_S^i with SD of ~0.34 K (cf. analyses in Section 3). For comparison, these numbers for de-biased CNLR SST estimate $T_S(\mathbf{a})$, produced using Eq. (5), are much greater: $\sigma[T_S(\mathbf{a}) - T_S^0] = 0.54$ K and $\sigma[T_S(\mathbf{a}) - T_S^i] = 0.49$ K. Two observations can be made here. First, low SNR typical for incremental regressors prevents obtaining a realistic measure of SST variability from incremental considerations alone. Therefore, an external measure of SST variability is needed to adjust the IncR coefficients. Second, precision of fitting in situ SST cannot be taken as an ultimate measure of the performance of any incremental SST algorithm because small value of $\sigma[T_S - T_S^i]$ can be achieved by simply using small coefficients in the algorithm equation (or even zero coefficients, which is equivalent to taking T_S^0 as a solution). This conclusion is important for validation and especially for intercomparison of incremental SST algorithms.

Within the scope of this study, the most reliable external measure of variability in SST increments can be obtained from CNLR SST. To preserve sensitivity of IncR SST to true SST increments, we scale $\mathbf{b_{LS}}$ in such a way as to equalize SD of IncR SST minus T_S^0, $\sigma[T_S(\mathbf{b}) - T_S^0]$, with similar SD for the CNLR SST, $\sigma[T_S(\mathbf{a}) - T_S^0]$ (note that $\sigma[T_S(\mathbf{b}) - T_S^0]$ and $\sigma[T_S(\mathbf{a}) - T_S^0]$ are produced according to Eq. (9), by averaging over all clear-sky SEVIRI observations in July 2008 within the entire retrieval domain):

$$\mathbf{b} = \alpha \mathbf{b_{LS}}, \tag{17}$$

$$\alpha = \left\{\sigma\left[T_S(\mathbf{a}) - T_S^0\right] / \sigma\left[T_S(\mathbf{b_{LS}}) - T_S^0\right]\right\}. \tag{18}$$

Here, $\alpha \approx 4.48$ is the scaling factor, $T_S(\mathbf{a})$ is CNLR SST estimate, according to Eq. (5). The scaling increases variability of IncR SST

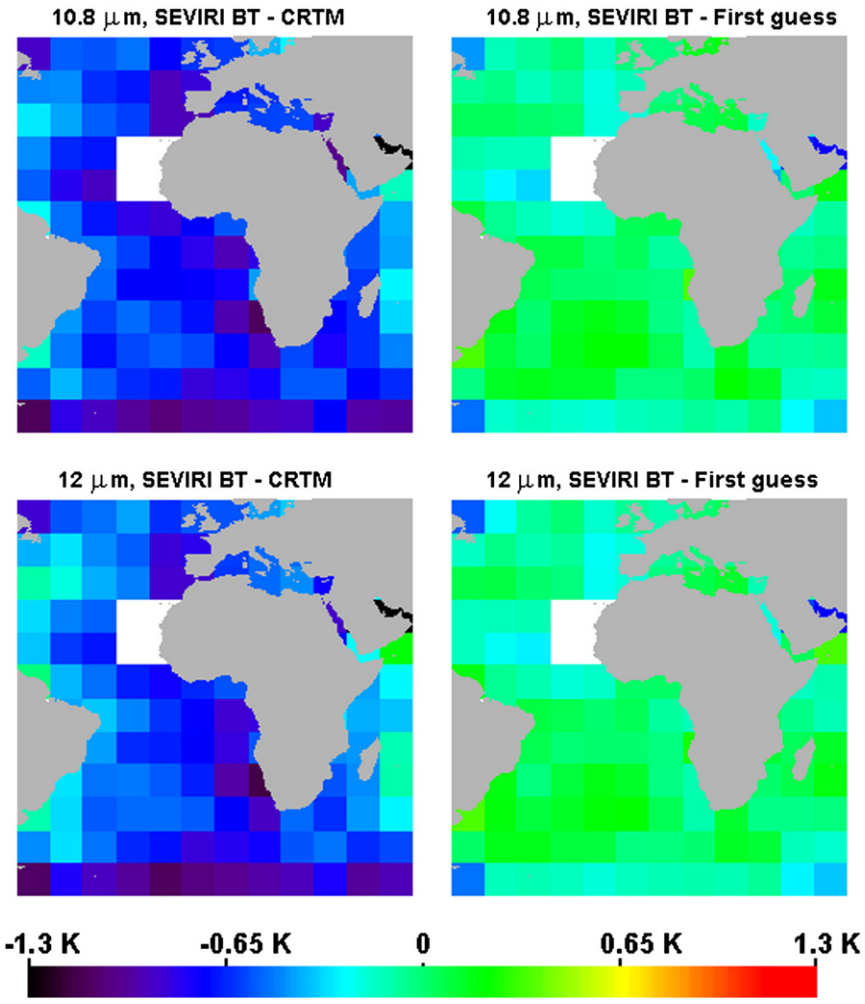

Fig. 3. Biases of (left panels) SEVIRI BT−CRTM and (right panels) SEVIRI BT-first guess, averaged over 10°×10° lat/lon cells for all nighttime clear-sky measurements in June 2008. (See also statistical summaries in Table 3).

increments, while preserving their correlation with in situ SST increments.

Table 4 compares the NLR and scaled IncR coefficients, appearing in front of similar regressors in Eqs. (1) and (6). (Recall that the CNLR algorithm uses the NLR coefficients.) Unlike the NLR equation (1), in which the offset a_0 is significant, the offset b_0 in the IncR Eq. (6) is small, suggesting that $T_S \approx T_S^0$ when $T_{B11} = T_{B11}^0$ and $T_{B12} = T_{B12}^0$. The scaled IncR coefficients b_1 and b_2 compare well with the corresponding NLR coefficients a_1 and a_2, whereas the coefficient b_3 in front of the VZA-dependent regressor in Eq. (6) significantly deviates from the NLR coefficient a_3. The relatively large positive value of a_3 indicates a pronounced sensitivity of NLR (and CNLR) SST to

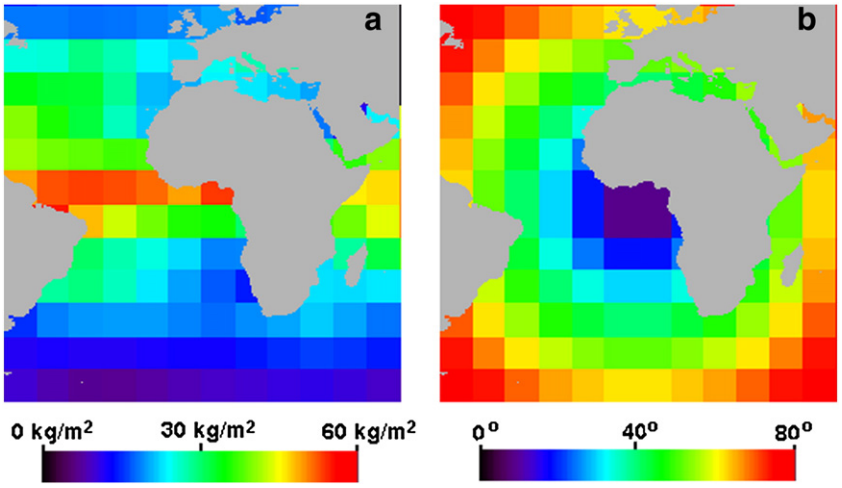

Fig. 4. The values of (a) TPW and (b) VZA averaged over 10°×10° lat/lon cells in June 2008.

Table 3
Mean and SD of regional biases of SEVIRI−CRTM BTs ($T_B - T_B^{CRTM}$) and SEVIRI−first-guess BTs ($T_B - T_B^0$) in channels 10.8 and 12 μm (from Fig. 3).

	10.8 μm		12 μm	
	Mean (K)	SD (K)	Mean (K)	SD (K)
$T_B - T_B^{CRTM}$	−0.665	0.220	−0.580	0.265
$T_B - T_B^0$	−0.043	0.168	−0.044	0.166

variations in BT increments at large VZA, whereas the sensitivity of IncR SST is suppressed as manifested by a significantly smaller value of b_3. The difference between a_3 and b_3 values can be due to the fact that the angular dependence of IncR regressors is reduced by subtracting first guess BTs from observed BTs. This reduces the load on the VZA-dependent term in Eq. (6) compared to Eq. (1). Note also that the sign of b_3 is negative and opposite to the signs of b_1 and b_2.

The method of calculation of IncR coefficients, described in this Section, suggests that, despite relatively low SNR, the incremental regressors still carry enough information to provide significant correlation between retrieved and in situ SST increments. Future development of the IncR approach can include further specification of the IncR coefficients using, for example, RTM considerations.

6. Implementation of the OE algorithm

The OE solution is produced by inverting a set of equations, which combines RTM and a priori information (e.g., Rodgers, 1976). To retrieve SST from two split window channels, OE requires two-dimensional parameterization of RTM with SST and one additional variable to account for variations in the atmospheric transmission. In our implementation of OE with SEVIRI channels 10.8 and 12 μm, the second retrieved variable is the Optical Depth Scaling Factor (ODSF), β, defined as a ratio of optical depth of water vapor absorption τ to its a priori estimate τ_0, computed from GFS data:

$$\beta = \tau/\tau_0. \tag{19}$$

The OE solution is constructed as:

$$\mathbf{z} = \mathbf{z^0} + \left(\mathbf{K}^T\Delta^{-1}\ \mathbf{K} + \mathbf{S}^{-1}\right)^{-1}\mathbf{K}^T\Delta^{-1}\left(\mathbf{T_B} - \mathbf{T_B^0}\right). \tag{20}$$

Here, $\mathbf{z} = [T_S, \beta]^T$ is a vector of unknown variables; $\mathbf{z^0} = [T_S^0, 1]^T$ is the first guess for $\mathbf{z}$; $\mathbf{T_B} = [T_{B11}, T_{B12}]^T$ is a vector of observed BTs; $\mathbf{T_B^0} = [T_{B11}^0, T_{B12}^0]^T$ is a vector of first-guess BTs; $\mathbf{K}$ is Jacobian (i.e., the matrix of derivatives of the CRTM function at 10.8 and 12 μm with respect to T_S and β); $\mathbf{S}$ is a covariance matrix of a priori distribution of $\mathbf{z}$; $\mathbf{\Delta}$ is a covariance matrix of radiometric noise in BTs. The elements of $\mathbf{K}$ are numerically computed along with T_B^{CRTM} on the GFS grid and interpolated to SEVIRI pixels. When computing BT derivatives with respect to β, profiles of atmospheric humidity are scaled proportionally at all atmospheric levels. The OE algorithm requires specifying the second moments of a priori statistical distributions for instrumental noise ($\mathbf{\Delta}$) and retrieved variables ($\mathbf{S}$). To simplify the process of OE adjustment, we followed Merchant et al. (2009a) and assumed that radiometric noise in both channels is independent, with equal RMS values, which corresponds to a diagonal matrix $\mathbf{\Delta}$, with equal diagonal elements η. Under this assumption, Eq. (20) is rewritten as:

$$\mathbf{z} = \mathbf{z^0} + \left(\mathbf{K}^T\mathbf{K} + \eta\mathbf{S}^{-1}\right)^{-1}\mathbf{K}^T\left(\mathbf{T_B} - \mathbf{T_B^0}\right). \tag{21}$$

The only term in Eq. (21), which depends on the second moments of a priori statistical distributions of noise and unknown variables, is $\eta\mathbf{S}^{-1}$. This allows fixing η at a certain value (we set η to 0.04 K^2, assuming that RMS noise value is 0.2 K) and adjusting only $\mathbf{S}$ elements. The non-diagonal elements of $\mathbf{S}$ were set to zero, assuming that T_S and β increments are statistically independent.

The most challenging part of OE implementation is the selection of diagonal elements of $\mathbf{S}$, σ_{SST} and σ_β, which are squares of a priori SD for T_S and β. The OE theory (e.g., Rodgers, 1976) suggests setting σ_{SST} and σ_β from a priori information. The DSST data set includes the Estimated SST Error Standard Deviation (ESD), which does not exceed 0.3 K for most of the area observed by SEVIRI. In the initial OE version, σ_{SST} was set to ESD interpolated to the sensor's pixels, and σ_β was set to 0.2. Similar to SST produced with the NLR using least-squares estimates of coefficients, the SST produced with this initial OE version fit in situ SST quite precisely, with $\sigma(T_S - T_S^i) = 0.37$ K and only slightly deviated from T_S^0, with $\sigma(T_S - T_S^0) = 0.23$ K. (Note

Table 4
Coefficients for Non-Linear Regression (NLR) and Incremental Regression (IncR).

Coefficient	Regressor	Value
NLR		
a_0	Offset	11.121
a_1	T_{B11}	0.96687
a_2	$(T_{B11} - T_{B12})(T_S^0 - 273.15)$	0.069788
a_3	$(T_{B11} - T_{B12})(sec\theta - 1)$	0.80178
IncR		
b_0	Offset	−0.032284
b_1	$T_{B11} - T_{B11}^0$	0.97533
b_2	$[(T_{B11} - T_{B11}^0) - (T_{B12} - T_{B12}^0)](T_S^0 - 273.15)$	0.084647
b_3	$[(T_{B11} - T_{B11}^0) - (T_{B12} - T_{B12}^0)](sec\theta - 1)$	−0.13250

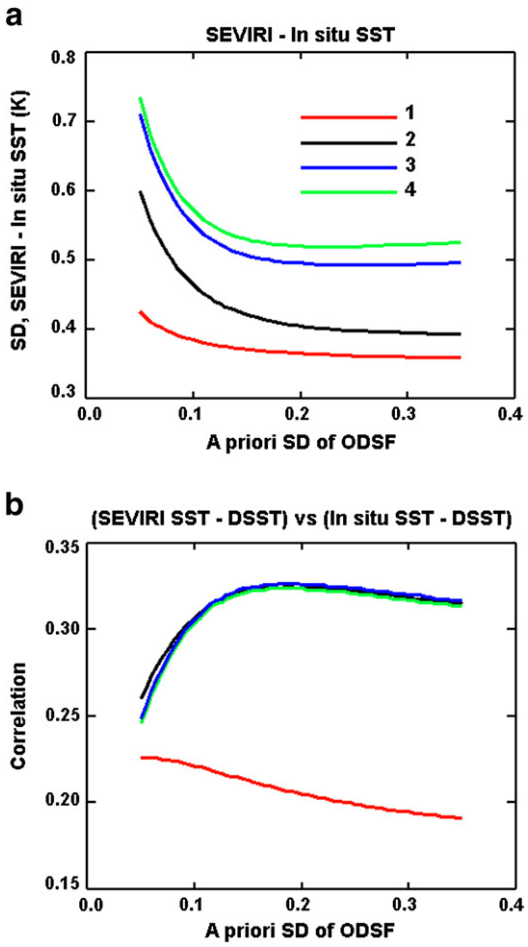

Fig. 5. (a) SD of OE−in situ SST and (b) correlation between increments (OE SST−DSST) and (in situ SST−DSST) as functions of a priori SD of ODSF. The curves correspond to different SD of a priori SST errors: 1 — spatially variable SD is taken from the DSST dataset (typically less than 0.3 K), 2 — 1 K; 3 — 2.14 K; 4 — 2.5 K.

Table 5
Statistics of SSTs retrieved with Non-Linear Regression (NLR), Corrected Non-Linear Regression (CNLR), Incremental Regression (IncR) and Optimal Estimation (OE) with respect to DSST and in situ SST. The statistics were averaged over the entire retrieval domain in June 2008.

Statistics	NLR	CNLR	IncR	OE
Retrieved SST−DSST				
$M(T_S-T_S^0)$ (K)	−0.058	0.011	−0.021	0.003
$\sigma(T_S-T_S^0)$ (K)	0.569	0.538	0.538	0.538
Retrieved SST−in situ SST				
$M(T_S-T_S^i)$ (K)	0.000	0.038	0.000	0.021
$\sigma(T_S-T_S^i)$ (K)	0.571	0.489	0.467	0.504
Incremental correlation				
$r(T_S-T_S^0, T_S^i-T_S^0)$	0.291	0.336	0.348	0.326

that a similar underestimation of true SST variations by OE was earlier reported by Merchant et al., 2009a.) An additional indication of the insufficiency of this initial OE version is a relatively low average correlation of retrieved SST increments with in situ SST increments, $r(T_S-T_S^0, T_S^i-T_S^0)=0.205$. In order to increase the range of retrieved SST increments, and to improve their correlation with in situ SST increments, in the final OE version σ_{SST} and σ_β were set to constant values, selected from the following consideration. Fig. 5a shows $\sigma(T_S-T_S^i)$ as a function of σ_β for the initial OE version and for three constant values of σ_{SST}. For $\sigma_{SST}>2$ K and $\sigma_\beta<0.2$, $\sigma(T_S-T_S^i)$ decreases as σ_β increases until it stabilizes itself at $\sigma_\beta\approx0.2$. Fig. 5b additionally shows that the correlation between $T_S-T_S^0$ and $T_S^i-T_S^0$ reaches its maximum near the same value of $\sigma_\beta=0.2$, within a wide range of σ_{SST}. Based on this result, the value of σ_β in the final OE version was set to 0.2. The value of σ_{SST} was set to 2.14 K to equalize $\sigma(T_S-T_S^0)$ for OE and CNLR.

7. Comparison of SST algorithms

Statistics of retrieved SST, averaged over the full retrieval domain in June 2008, are shown in Table 5 for four algorithms. SD of retrieved SST minus DSST, $\sigma(T_S-T_S^0)$, characterizes variability of retrieved SST increments. Recall that for IncR and OE, $\sigma(T_S-T_S^0)$ was equalized to that of CNLR. For CNLR SST, $\sigma(T_S-T_S^0)$ is smaller than for NLR, due to subtraction of regional biases, according to Eq. (3). Removal of regional biases from CNLR SST also reduces SD of retrieved minus in situ SST, $\sigma(T_S-T_S^i)$ (consistent with Le Borgne et al., 2011) and increases incremental correlation, $r(T_S-T_S^0, T_S^i-T_S^0)$, compared with NLR. The IncR further reduces $\sigma(T_S-T_S^i)$ and increases $r(T_S-T_S^0, T_S^i-T_S^0)$ due to optimization of regression coefficients specifically for incremental retrieval. The OE demonstrates higher $\sigma(T_S-T_S^i)$ and lower $r(T_S-T_S^0, T_S^i-T_S^0)$ than CNLR and IncR. Recall that this result is the best case scenario for the OE, which was adjusted to maximize $r(T_S-T_S^0, T_S^i-T_S^0)$.

Fig. 6 shows maps of retrieved SST minus DSST, produced from a single SEVIRI image, taken at 00:00 UTC on June 2, 2008 with four SST algorithms. The CNLR, IncR, and OE SST images reproduce similar large-scale SST anomalies whereas NLR SST is noticeably subject to the effect of large regional biases.

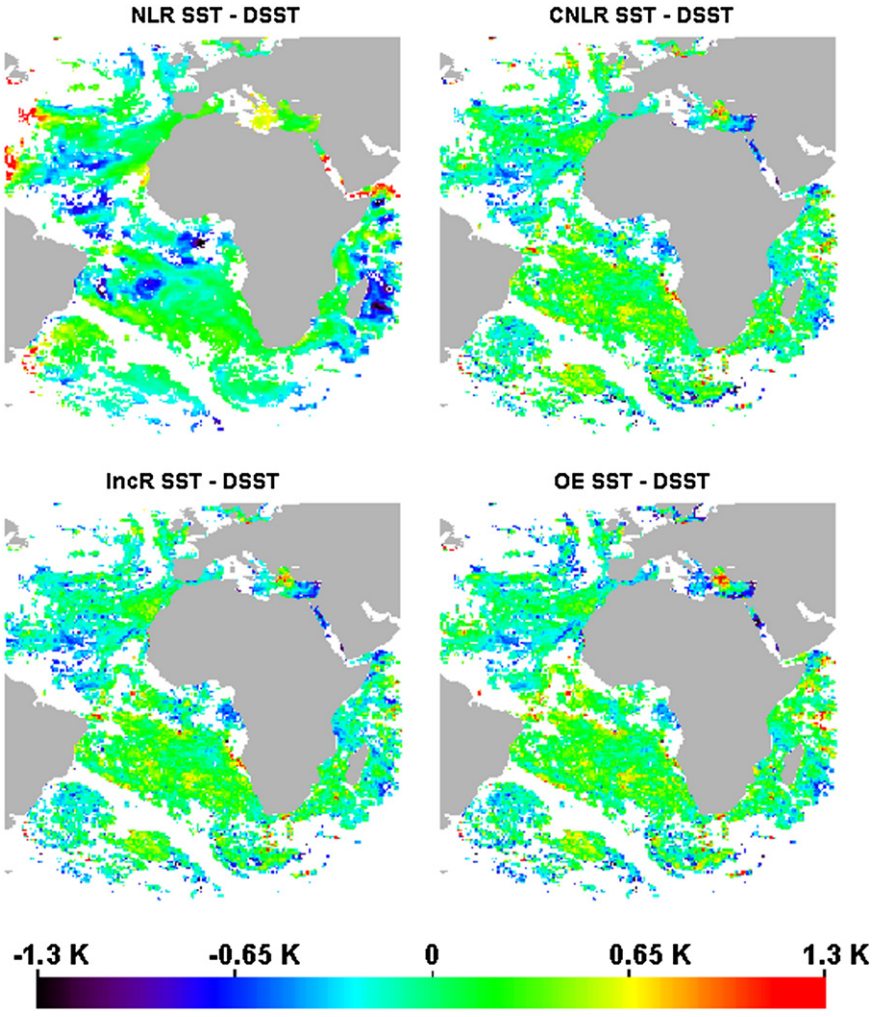

Fig. 6. Maps of SEVIRI SST−DSST produced with four algorithms from the SEVIRI image taken at 00 UTC on June 2, 2008.

Fig. 7 demonstrates statistics of retrieved SST minus in situ SST as functions of VZA and TPW, averaged over nighttime clear-sky SEVIRI pixels in June 2008. NLR biases in Fig. 7a–b vary with greater magnitudes compared to all incremental algorithms. Negative bias in NLR SST is especially pronounced at TPW>40 kg/m^2. At the same time, SST biases for CNLR, IncR, and OE algorithms vary within ± 0.1 K. Therefore, one concludes that any type of incremental SST algorithm, which uses debiased first guesses for BTs, allows efficient correction of regional biases typical for NLR SST.

Fig. 7c–d show $\sigma(T_S - T_S^i)$ as functions of VZA and TPW. The values of $\sigma(T_S - T_S^i)$ are largest and the dependencies are most non-uniform for the NLR. The IncR SST provides the most uniform $\sigma(T_S - T_S^i)$ within the full range of VZAs and the lowest $\sigma(T_S - T_S^i)$ at VZA>40°, where the number of matchups is largest (cf. Fig. 1a). As a result, $\sigma(T_S - T_S^i)$ for IncR SST is lowest at all TPWs in Fig. 7d. The fact that the IncR improves SST precision at large VZAs is especially important because it extends the domain in which accurate SST retrievals are possible. Note that the IncR algorithm shows relatively small $\sigma(T_S - T_S^i)$ at larger VZAs and TPWs, where the atmospheric absorption grows and observed BTs become more sensitive to variations in the atmospheric transmission rather than in SST (e.g., Aoki, 1979). For CNLR SST, superior performance in high atmospheric absorption conditions is also observed, although the improvement is less pronounced. For the OE SST, $\sigma(T_S - T_S^i)$ at VZA>50° and especially at TPW>40 kg/m^2 is greater than for CNLR and IncR. However, at near-nadir VZA<40°, $\sigma(T_S - T_S^i)$ of OE SST is smallest of all algorithms, but this improvement is achieved at the expense of the most non-uniform angular dependence of $\sigma(T_S - T_S^i)$ among the three incremental algorithms.

The incremental correlations as functions of VZA and TPW are shown in Fig. 7e–f. For all four algorithms, maximum values of $r(T_S - T_S^0, T_S^i - T_S^0)$ and minimum values of $\sigma(T_S - T_S^i)$ take place within the range of VZA from 10° to 30° and within the range of TPW from

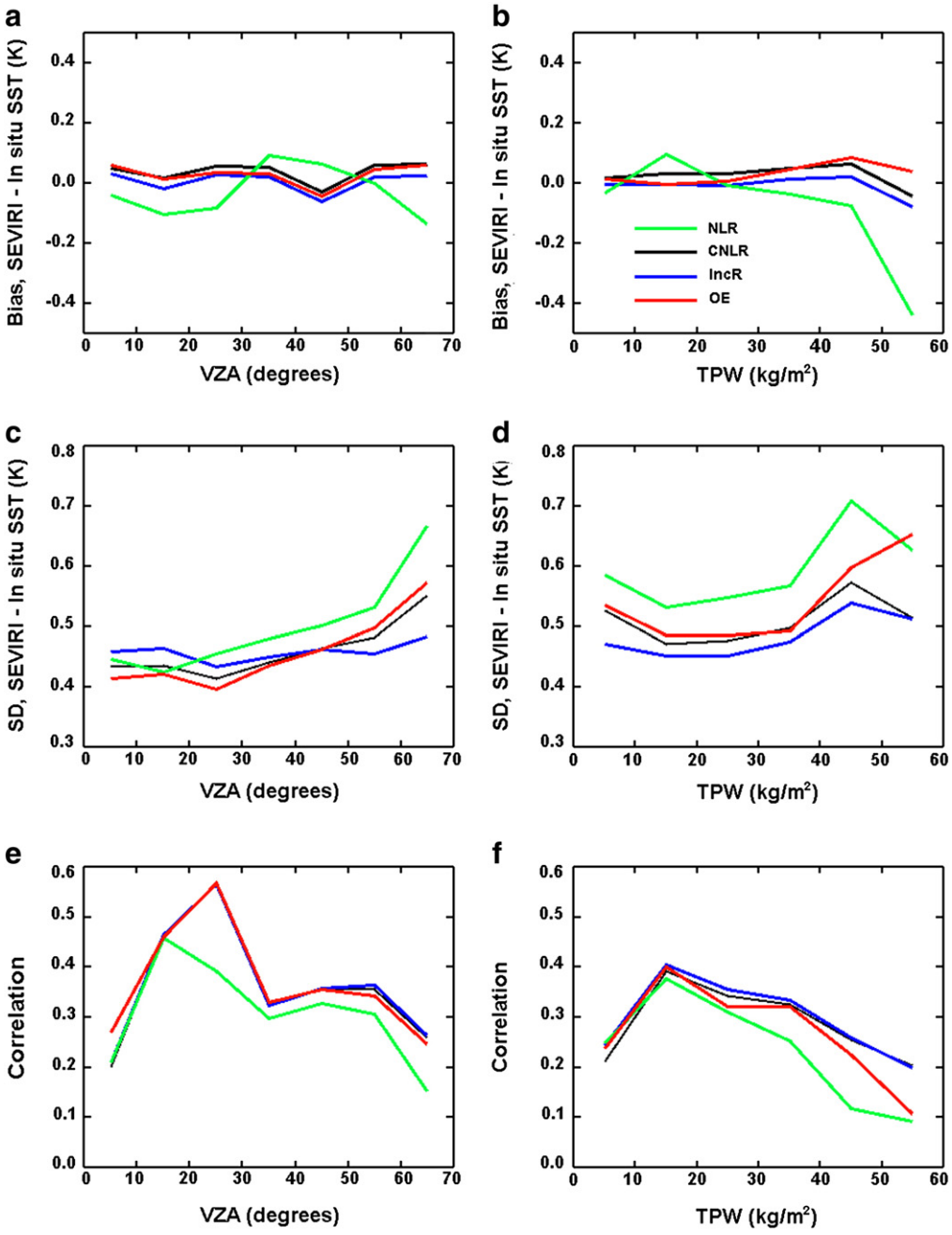

Fig. 7. (a,b) Biases of retrieved − in situ SST, (c,d) SD of retrieved − in situ SST, (e,f) correlations (retrieved SST−DSST) and (in situ SST−DSST) as functions of (a,c,e) VZA and (b,d,f) TPW.

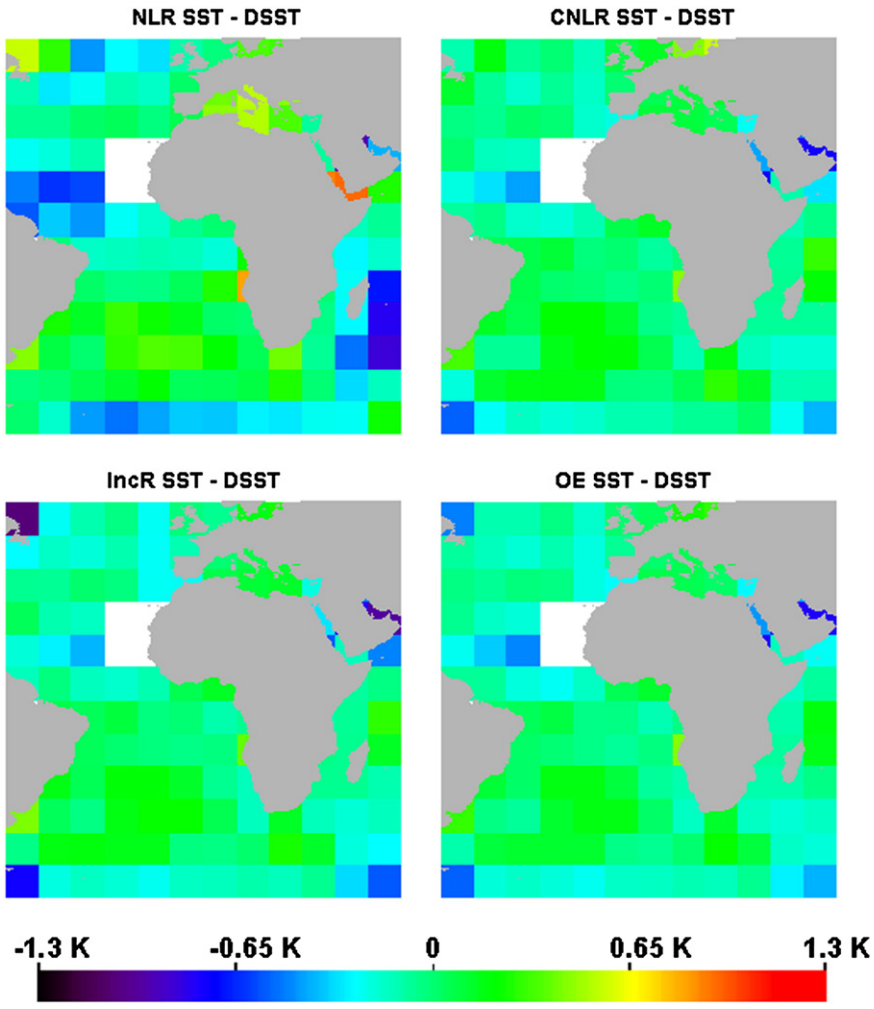

Fig. 8. Biases of SEVIRI SST−DSST, averaged over 10°×10° lat/lon cells, as produced with four SST algorithms. (See also statistical summaries in Table 6.).

10 kg/m^2 to 30 kg/m^2. Correlations for NLR SST are generally lower than for incremental algorithms. Overall, the IncR algorithm shows a small yet statistically significant increase of incremental correlation compared with CNLR and OE within VZA range >40° and 10 kg/m^2 ≤ TPW ≤ 40 kg/m^2, which correspond to the maximum number of matchups (cf. Fig. 1a–b).

Fig. 8 shows geographical distributions of regional biases in retrieved SST minus DSST, averaged over 10°×10° latitudinal/longitudinal cells in June 2008. The magnitude of variations in regional NLR SST biases is greater than for the incremental algorithms. Locations and signs of major NLR SST biases in Fig. 8a (negative bias north of the Equator and positive biases at the southwest African coast, in the Mediterranean, and in the South Atlantic) are consistent with those reported by Le Borgne et al. (2011), who implemented the CNLR using a different form of the NLR equation, RTM, and input fields. In particular, they used Operational Sea Surface Temperature and Sea Ice Analysis (OSTIA, Stark et al., 2008) as a reference SST field, RTTOVS-9 (Saunders et al., 2008), and atmospheric profiles from the European Center for Medium-range Weather Forecasting (ECMWF). The consistency of our results with results by Le Borgne et al. (2011) can be considered as an independent verification of the superior performance of the CNLR over the NLR. Fig. 8a also demonstrates greater NLR SST biases (mainly negative) at larger VZAs. The regional biases for all the incremental algorithms in Fig. 8b–d are more uniform in space. Table 6 additionally quantifies data shown in Fig. 8. For all four algorithms, the mean values of regional biases are between −0.1 K and 0 K. Variability of regional biases is characterized with their SD averaged (in a root-mean-square sense) within the retrieval domain. This SD is lowest for the IncR algorithm (~0.20 K) and highest for NLR (~0.35 K). Note that the DSST field itself may include regional biases with respect to true SST, thus contributing to the variability of regional biases in retrieved SST minus DSST. For reference, Table 6 also shows mean and SD of regional differences between two analysis fields, OSTIA and DSST, averaged during June 2008 over the retrieval domain. The latter SD, which can be viewed as an upper estimate of uncertainty of regional biases in DSST minus true SST, is much lower than that for NLR SST and somewhat higher than for any of the incremental algorithms. This suggests that the incremental SST algorithms are capable of reducing the a priori uncertainty in the first guess SST field.

Regional variability of retrieved SST increments is characterized in Fig. 9 with SDs of $T_S - T_S^0$, $\sigma_{cell}(T_S - T_S^0)$, averaged within each 10°×10° cell. Consistently with Fig. 7c–d, the geographic distribution of $\sigma_{cell}(T_S - T_S^0)$ is least uniform for NLR SST and most uniform for IncR SST. The

Table 6
Top two rows: mean and SD regional SST biases with respect to DSST averaged over 10°×10° cells (from Fig. 8). Bottom row: mean (in root-mean-square sense) regional SDs of retrieved SST minus DSST (from Fig. 9).

	NLR	CNLR	IncR	OE	OSTIA
Mean regional bias	−0.051	−0.048	−0.085	−0.083	−0.033
SD of regional biases	0.348	0.216	0.199	0.234	0.248
Mean regional SD	0.675	0.570	0.517	0.612	–

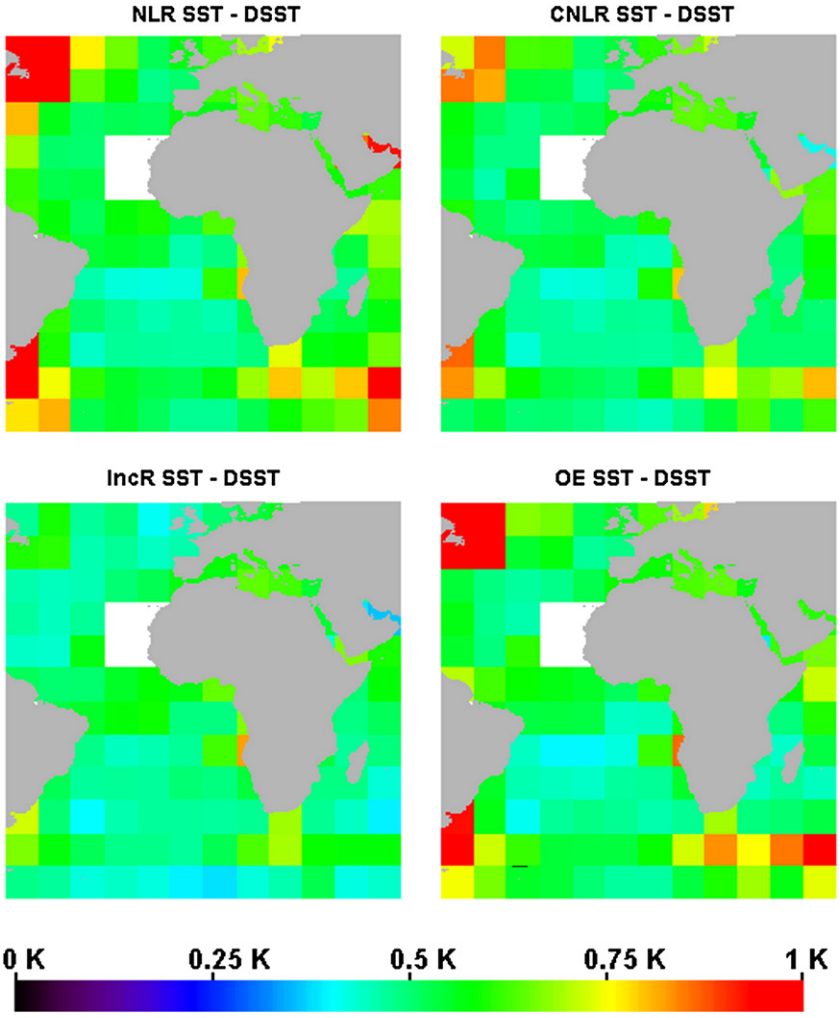

Fig. 9. SDs of SEVIRI SST−DSST, averaged over 10°×10° lat/lon cells, as produced with four SST algorithms. (See also statistical summaries in Table 6.).

bottom row in Table 6 shows average (in a root-mean-square sense) values of $\sigma_{cell}(T_S - T_S^0)$ over all 10°×10° cells. The average $\sigma_{cell}(T_S - T_S^0)$ is smallest for the IncR algorithm, suggesting that the IncR minimizes average regional variability of retrieved SST increments.

8. Conclusion and future work

All tested incremental SST algorithms are capable of reducing regional SST biases typical for split-window Non-Linear Regression, provided that regional biases in simulated first-guess BTs with respect to observed BTs are removed prior to SST retrieval. In this study, correction of BT biases was performed consistently and uniformly for all incremental algorithms, allowing comparison of their performance. The incremental algorithms also reduce SD of retrieved minus in situ SST over the NLR. The CNLR significantly improves SST accuracy and precision compared with NLR due to correction for regional biases (Eq. 3) in the conventional NLR SST. The adjustment of regression coefficients within the IncR resulted in further improvement of overall SST precision and in more uniform dependencies of SST precision on VZA and TPW. This also minimized variability of regional IncR SST biases. The OE, as it was implemented in this study, underperformed CNLR and IncR in terms of overall statistics of retrieved SST, as well as the magnitude of regional SST biases. It is possible, that the performance of the OE can be further improved by a different parameterization of RTM, further specification of the inverse operator, or more accurate calculation of the RTM Jacobian. However, adjustment of OE is evidently a more ambiguous and uncertain process than calculation of IncR coefficients.

An important result of this study is that adjustment and validation of incremental SST algorithms require methodology different from the conventional approach, in which SD of fitting in situ SST is considered as the only and ultimate criterion of the performance of an SST algorithm. An additional constraint should be imposed on variability of retrieved SST increments based on certain a priori information on true SST increments. In the case of IncR, this information is needed to scale initial estimates of regression coefficients, which are biased due to low SNR of incremental regressors. In the case of OE, this information allows balancing observations and a priori information — the problem similar to choosing a regularization parameter in ill-posed inverse problems (e.g., Tikhonov & Arsenin, 1977). When it comes to validation of incremental SST algorithms, it should be taken into account that precise fitting of in situ SST with retrieved SST can be achieved simply by forcing the solution to the first guess. Therefore, comparison of incremental algorithms in terms of precision of fitting in situ SST also requires controlling variability of retrieved SST increments. It appears to be useful to compare incremental SST algorithms in terms of correlation of retrieved and in situ SST increments. As shown in Section 7, incremental correlation is capable of showing the difference in real contributions of true SST variations to variations in SST retrieved with different algorithms.

Based on the algorithm comparisons documented here, the Incremental Regression was recommended as the baseline SST algorithm

for GOES-R ABI. Future work on the IncR algorithm will include optimization of the retrieval equation, exploring alternative ways of BT bias correction and derivation of IncR coefficients and their testing using independent datasets, and during extended time periods.

Acknowledgments

This work was conducted under the Algorithm Working Group (AWG) funded by the GOES-R Program Office. We thank the AWG Managers, Drs. Mitch Goldberg and Jaime Daniels, and our colleagues John Sapper (NESDIS/OSPO), XingMing Liang, Feng Xu, Prasanjit Dash (STAR/CIRA), John Stroup (STAR/SSAI), and Denise Frey (OSPO/DPGS) for their valuable assistance, discussions, and feedback at different stages of work. We also thank Professor Peter Minnett, and three anonymous reviewers of this manuscript, for their very constructive recommendations which greatly helped us to rethink and rewrite the text. The views, opinions, and findings contained in this paper are those of the authors and should not be construed as an official NOAA or US Government position, policy, or decision.

References

Aoki, T. (1979). On the information content of the satellite measured infrared radiation in the atmospheric window region. *Journal of the Meteorological Society of Japan*, *57*, 73–78.

Brisson, A., Le Borgne, P., & Marsouin, A. (2002). Result of one year of preoperational production of Sea Surface temperatures from GOES-8. *Journal of Atmospheric and Oceanic Technology.*, *19*(10), 1638–1652.

Donlon, C. J., Minnett, P. J., Gentemann, C., Nightingale, T. J., Barton, I. J., Ward, B., et al. (2002). Toward improved validation of satellite sea surface skin temperature measurements for climate research. *Journal of Climate*, *15*, 353–369.

Gemmill, W., Katz, B., & Li, X. (2007). Daily real-time, global sea surface temperature–high resolution analysis: RTG_SST_HR. NCEP/EMC Office note. http://polar.ncep.noaa.gov/mmab/papers/on260/sst_office_note.pdf

Han, Y., Van Delst, P., Liu, Q., Weng, F., Yan, B., & Derber, J. (2005). User's guide to the JCSDA community radiative transfer model (beta version), NOAA/NASA/JCSDA. http://www.star.nesdis.noaa.gov/smcd/spb/CRTM/crtm-code/CRTM_UserGuide-beta.pdf

Ignatov, A., Petrenko, B., Shabanov, N., Kihai, Y., Dash, P., Liang, X., et al. (2010). *GOES-R Advanced Baseline Imager (ABI) algorithm theoretical basis document for sea surface temperature.* : NOAA NESDIS Center for Satellite Applications and Research, http://goesrtest2.woc.noaa.gov/products/ATBDs/baseline/SST_v2.0.pdf

Kawai, Y., & Wada, A. (2007). Diurnal SST variation and its impact on the atmosphere and ocean: A review. *Journal of Oceanography*, *63*, 721–744.

Khattak, S., Vaughan, R. A., & Cracknell, A. P. (1991). Sunglint and its observation in AVHRR data. *Remote Sensing of Environment*, *37*, 101–116.

Le Borgne, P., Roquet, H., & Merchant, C. J. (2011). Estimation of sea surface temperature from the Spinning Enhanced Visible and Infrared Imager, improved using numerical weather prediction. *Remote Sensing of Environment*, *115*, 55–65.

Liang, X., Ignatov, A., & Kihai, Y. (2009). Implementation of the Community Radiative Transfer Model (CRTM) in Advanced Clear-Sky Processor for Oceans (ACSPO) and validation against nighttime radiances. *Journal of Geophysical Research*, *114*, D06112, doi:10.1029/2008JD010960.

Liang, X., and Ignatov, A. (in press). Monitoring of IR Clear-sky Radiances over Oceans for SST (MICROS). *Journal of Atmospheric and Oceanic Technology*.

Maturi, E., Harris, A., Merchant, C., Mittas, J., Potash, B., Meng, W., et al. (2008). NOAA's sea surface temperature products from operational geostationary satellites. *Bulletin of the American Meteorological Society*, *89*, 1877–1888.

McClain, E. P., Pichet, W. G., & Walton, C. C. (1985). Comparative performance of AVHRR-based multichannel sea-surface temperatures. *Journal of Geophysical Research*, *90*, 1587–1601.

Merchant, C. J., Embury, O., Le Borgne, P., & Bellee, B. (2006). Saharan dust in nighttime thermal imagery: Detection and reduction of related biases in retrieved sea surface temperature. *Remote Sensing of Environment*, *104*, 15–30.

Merchant, C. J., Le Borgne, P., Marsouin, A., & Roquet, H. (2008). Optimal estimation of sea surface temperature from split window observations. *Remote Sensing of Environment*, *112*, 445–457.

Merchant, C. J., Le Borgne, P., Roquet, H., & Marsouin, A. (2009a). Sea surface temperature from a geostationary satellite by optimal estimation. *Remote Sensing of Environment*, *113*, 445–457.

Merchant, C. J., Harris, A. R., Roquet, H., & Le Borgne, P. (2009b). Retrieval characteristics of non-linear sea surface temperature from the Advanced Very High Resolution Radiometer. *Geophysical Research Letters*, *36*, L17604, doi:10.1029/2009GL039843.

Minnett, P. (2003). Radiometric measurements of the sea surface skin temperature: The competing roles of the diurnal thermocline and the cool skin. *International Journal of Remote Sensing*, *25*, 1197–1207.

O'Carroll, A. G., Eyre, J. R., & Saunders, R. W. (2008). Three-way error analysis between AATSR, AMSR-E and in situ sea surface temperature observations. *Journal of Atmospheric and Oceanic Technology*, *25*, 1197–1207.

Ostle, B., & Malone, L. C. (1988). *Statistics in research.* : Iowa State University Press 664 pp.

Petrenko, B., Ignatov, A., Kihai, Y., & Heidinger, A. (2010a). Clear-sky mask for the Advanced Clear-Sky Processor for Oceans. *Journal of Atmospheric and Oceanic Technology*, *27*, 1609–1623.

Petrenko, B., Ignatov, A., Shabanov, N., Kihai, Y., & Xu, F. (2010b). Hybrid SST Retrieval Algorithm in thermal IR: Combining regression and radiative transfer model approaches. *17th conference on satellite meteorology and oceanography, 26–30 September, Annapolis, MD.* http://ams.confex.com/ams/17Air17Sat9Coas/techprogram/paper_174578.htm

Reynolds, R. W., Smith, T. M., Liu, C., Chelton, D. B., Casey, K. S., & Schlax, M. G. (2007). Daily high-resolution-blended analyses for sea surface temperature. *Journal of Climate*, *20*, 5473–5496.

Rodgers, C. D. (1976). Retrieval of atmospheric temperature and composition from remote measurements of thermal radiation. *Reviews of Geophysics and Space Physics*, *14*, 609–624.

Saunders, R., Matricardi, M., Geer, A., Rayer, P., Embury, O., & Merchant, C. (2008). RTTOV-9 science and validation report. NWPSAF-MO-TV-020, 1. http://research.metoffice.gov.uk/research/interproj/nwpsaf/rtm/rttov9_files/rttov9_svr.pdf

Schmetz, J., Pill, P., Tjemkes, S., Just, D., Kerkmann, J., Rota, S., et al. (2002). An introduction to Meteosat Second Generation (MSG). *Bulletin of the American Meteorological Society*, *83*, 977–992.

Schmit, T. J., Gunshor, M. M., Menzel, W. P., Gurka, J. J., Li, J., & Bachmeier, A. S. (2005). Introducing the next-generation Advanced Baseline Imager on GOES-R. *Bulletin of the American Meteorological Society*, *86*, 1079–1096.

Shabanov, N., Ignatov, A., Petrenko, B., Kihai, Y., Liang, X., Guo, W., et al. (2009). Prototyping SST retrievals from GOES-R ABI with MSG SEVIRI data. *Fifth annual symposium on future operational environmental satellite systems — NPOESS and GOES-R, 11–15 January 2009, Phoenix, AZ.* http://ams.confex.com/ams/89annual/techprogram/paper_143903.htm

Shabanov, N., Ignatov, A., Petrenko, B., Kihai, Y., & Heidinger, A. (2010). Integrated cloud mask and quality control for GOES-R ABI SST: Prototyping with MSG/SEVIRI. *Sixth annual symposium on future operational environmental satellite systems — NPOESS and GOES-R, 17–21 January 2010, Atlanta, GA.* http://ams.confex.com/ams/90annual/techprogram/paper_160582.htm

Stark, J. D., Donlon, C., & O'Carroll, A. (2008). Determination of AATSR biases using the OSTIA SST analysis system and a matchup database. *Journal of Atmospheric and Oceanic Technology*, *25*, 1208–1217.

Swap, R., Ulanski, S., Cobbett, M., & Garstang, M. (1996). Temporal and spatial characteristics of Saharan dust outbreaks. *Journal of Geophysical Research*, *101*, 4205–4220.

Tikhonov, A., & Arsenin, V. (1977). *Solution of ill-posed problems.* New York: Wiley.

Walton, C. C., Pichel, W. G., Sapper, J. F., & May, D. A. (1998). The development and operational application of nonlinear algorithms for the sea surface temperatures with the NOAA polar-orbiting environmental satellites. *Journal of Geophysical Research*, *103*, 27999–28012.

Wu, X., Menzel, W. P., & Wade, G. S. (1999). Estimation of sea surface temperatures using GOES-8/9 radiance measurements. *Bulletin of the American Meteorological Society*, *80*, 1127–1138.

Xu, F., & Ignatov, A. (2010). Evaluation of in situ SSTs for use in the calibration and validation of satellite retrievals. *Journal of Geophysical Research*, *115*, C09022. http://www.star.nesdis.noaa.gov/sod/sst/iquam/images/Xu_Ignatov_2009_submitted_JGR.pdf, doi:10.1029/21010JC006129

Xu, F. & A. Ignatov (submitted for publication). Quality Control and Monitoring of *in situ* SST for Satellite Applications. *Journal of Atmospheric and Oceanic Technology*.